Bioinspired co-crystals of Imatinib providing enhanced kinetic solubility

Maude Reggane[a], Johannes Wiest[b], Marco Saedtler[b], Cornelius Harlacher[a], Marcus Gutmann[b], Sven H. Zottnick[c], Philippe Piechon[a], Ina Dix[a], Klaus Müller-Buschbaum[c], Ulrike Holzgrabe[b], Lorenz Meinel[b,*], Bruno Galli[a]

[a] Novartis Pharma AG, Novartis Campus, CH-4056 Basel, Switzerland
[b] Institute for Pharmacy and Food Chemistry, University of Wuerzburg, Am Hubland, DE-97074 Wuerzburg, Germany
[c] Institute for Inorganic Chemistry, University of Wuerzburg, Am Hubland, DE-97074 Wuerzburg, Germany

ARTICLE INFO

ABSTRACT

Realizing the full potential of co-crystals enhanced kinetic solubility demands a comprehensive understanding of the mechanisms of dissolution, phase conversion, nucleation and crystal growth, and of the complex interplay between the active pharmaceutical ingredient (API), the coformer and co-existing forms in aqueous media. One blueprint provided by nature to keep poorly water-soluble bases in solution is the complexation with phenolic acids. Consequently, we followed a bioinspired strategy for the engineering of co-crystals of a poorly water-soluble molecule – Imatinib – with a phenolic acid, syringic acid (SYA). The dynamics of dissolution and solution-mediated phase transformations were monitored by Nuclear Magnetic Resonance (NMR) spectroscopy, providing mechanistic insights into the 60 fold-increased long lasting concentrations achieved by the syringate co-crystals as compared to Imatinib base and Imatinib mesylate. This lasting effect was linked to SYA's ability to delay the formation and nucleation of Imatinib hydrate – the thermodynamically stable form in aqueous media – through a metastable association of SYA with Imatinib in solution. Results from permeability studies evidenced that SYA did not impact Imatinib's permeability across membranes while suggesting improved bioavailability through higher kinetic solubility at the biological barriers. These results reflect that some degree of hydrophobicity of the coformer might be key to extend the kinetic solubility of co-crystals with hydrophobic APIs. Understanding how kinetic supersaturation can be shaped by the selection of an interactive coformer may help achieving the needed performance of new forms of poorly water-soluble, slowly dissolving APIs.

1. Introduction

Poorly water-soluble active pharmaceutical ingredients (API) frequently drive the need for complex enabling formulations including amorphous solid dispersions, lipid-based drug delivery systems, complexation with cyclodextrins, nanoparticles, and microemulsions [1,2]. Nature follows another strategy when challenged by low water solubility, e.g. when aromatic bases are kept in solution within plant vacuoles as part of a species defense armamentarium against pathogens and herbivores [3]. One blueprint provided by nature being of particular interest is the complexation of drugs with polyphenols [4]. For example, caffeine is complexed with chlorogenic acid in *Coffea arabica Linn.*, as first described in 1907 [5] and more recently detailed by 1D and 2D high resolution ^{1}H and [13]C Nuclear Magnetic Resonance (NMR) spectroscopy [6]. Cocaine is complexed to chlorogenic acid in the vacuoles of *Erythroxylum coca Lam.* with both interactions relying on overlaying π orbitals, hence π stacking of the API and the acid [7].

Consequently, we aimed for a biomimetic strategy to identify novel coformers to enhance the kinetic solubility of poorly water-soluble basic APIs. Indeed co-crystals are an attractive alternative to salt formation due to the large number of coformers available and the applicability to neutral APIs. Many designed salts and co-crystals reflect high energy forms generating supersaturated solutions [8]. Supersaturated states are ultimately unstable, but if the transient stabilization of these states is understood (i.e. detailed picture of the kinetics of nucleation and crystal growth) [9–12] it allows translation *in vivo* [13,14]. In particular co-crystals may have a higher stability in solution than salts due to the higher number of small scale intermolecular interactions between API and coformer. Forms that are stable in solution maintain high concentrations over time which drives diffusion through membranes. Here we hypothesized that association in solution via π stacking could temporarily stabilize supersaturated states as generated by high energy forms of APIs.

Imatinib – the first selective tyrosine-kinase inhibitor [15] – has a

flat molecular architecture along with aromaticity, thereby favoring π stacking in solution with other aromatic molecules such as phenolic acids, and was selected as a model compound. Syringic acid (SYA; a phenolic acid; 4-hydroxy-3,5-dimethoxybenzoic acid) which is naturally occurring in plants (e.g. *Euterpe oleracea Mart.* with concentrations exceeding 1 g/L in oil) [16], in fruits (e.g. strawberries contain more than 2 mg/kg) [17], and in wines (up to 8 mg/kg in red wine) [18] was selected as coformer. SYA's crystal structure was recently reported [19]. In addition to stacking interactions, the carboxylic acid and phenolic acid functional groups of SYA are likely to form the well known COOH···N or phenol OH···N supramolecular heterosynthons with one or several of Imatinib nitrogens, thus maximizing the interaction between the two species. To our knowledge, the acid has not been used as a counterion for salt formation or as coformer in co-crystals with APIs so far.

We followed a bioinspired approach using SYA for transient but kinetically stabilized supersaturated states of Imatinib. For that, we engineered and characterized co-crystals between SYA and Imatinib, studied the co-crystals dissolution kinetics and phase transformations, detailed the mechanisms of prolonged supersaturation, while assessing the impact of aggregation on diffusion through artificial and biological membranes.

2. Materials and methods

Imatinib free base (IFB) and Imatinib mesylate (IM) were provided by Novartis Pharma AG (Basel, Switzerland). Sodium chloride and potassium dihydrogen phosphate (EMSURE grade) used for buffer preparation, LiChropur formic acid and LiChrosolv acetonitrile used for mobile phases preparation, and EMSURE grade solvents used for crystallization were purchased from Merck (Darmstadt, Germany). Millipore water was obtained from a Milli-Q dispenser equipped with a Millipal Express 40 filter (0.22 μm) from Merck KGaA (Darmstadt, Germany). Penicillin G and streptomycin solutions were purchased from Biochrom AG (Berlin, Germany). Caco-2 cells were purchased from DSMZ GmbH (Braunschweig, Germany). Greiner Cellstar® 12-well culture plates and ThinCert™ cell culture inserts, 0.4 μm pore diameter, transparent were purchased from Greiner Bio-One GmbH (Frickenhausen, Germany). Fetal bovine serum (FBS) was purchased from Gibco (Darmstadt, Germany). Whatman® Puradisc 4 syringe filters, 0.2 μm, PVDF were purchased from VWR International GmbH (Darmstadt, Germany) and 0.45 μm PVDF centrifugal filters (Ultrafree MC HV) were purchased from Merck & Cie (Schaffhausen, Switzerland). Fluorescein sodium extra pure was purchased from Merck KGaA (Darmstadt, Germany). Methanesulfonic acid ≥99.5%, Syringic acid ≥95%, Propranolol hydrochloride ≥99%, HEPES BioPerformance Certified ≥99.5%, Lucifer Yellow CH dilithium salt, Hanks' Balanced Salt solution (HBSS), Dulbecco's modified Eagle's medium high glucose (DMEM), Non-essential Amino Acids solution 100x (NEAA), sodium phosphate monobasic monohydrate, and sodium phosphate dibasic heptahydrate were purchased from Sigma-Aldrich GmbH (Schnelldorf, Germany). Deuterated water (D_2O, 99.9% D) and deuterated aceticacid-d_4 (99.5% D) were purchased from Deutero GmbH (Kastellaun, Germany), 40% sodium deuteroxide in deuterated water (NaOD, 99% D), 35% deuterium chloride in deuterated water (DCl, 99% D), 85% deuterated phosphoric acid-d_3 in deuterated water (D_3PO_4, 98% D) and deuterated water (D_2O, 99.9% D) containing 0.05% 3-(trimethylsilyl) propionic-2,2,3,3-d4 acid-Na (TSP-d_4), sodium chloride (99%) and monobasic sodium phosphate anhydrous (99%) from Sigma-Aldrich (Schnelldorf, Germany), hexadeuteriodimethyl sulfoxide (DMSO-d_6, 99.8% D) from Euriso-top (Saarbrücken, Germany), monobasic sodium phosphate monohydrate (99%) from Gruessing (Filsum, Germany), dibasic sodium phosphate anhydrous (99%) from Acros Organics (Geel, Belgium) and Tween 80 from Caelo (Hilden, Germany). Standard 5 mm NMR tubes (400 MHz/900 MHz) and coaxial insert tubes were purchased from Norell (Landisville, PA).

3. Methods

3.1. Small scale screening

An initial small scale screening was performed to obtain Imatinib syringate co-crystal (referred to as I-SYA (1:1) co-crystal). A 1:1.1 stoichiometric mixture of IFB and SYA was weighted in a 16 × 130 cm Schott Duran test-glass (Mainz, Germany). 600 μL of ethanol were added and the mixture was heated to boiling point with a heat gun HL 2010 E from Steinel (Herzebrock-Clarholz, Germany) until complete dissolution. The solution was left on a Syncore orbital shaker from Büchi (Liestal, Switzerland) under light stirring conditions (100 rpm) at room temperature for 48 h. A thick precipitate was recovered, filtered and washed with two volumes of ethanol. I-SYA (1:1) co-crystal formation was confirmed by NMR, DSC, and XRPD.

3.2. Preparation of Imatinib co-crystals

I-SYA (1:1) and I-SYA (1:2) co-crystals at grams scale were prepared by cooling crystallization in an EasyMax 102 system from Mettler-Toledo (Greifensee, Switzerland). To prepare I-SYA (1:1) co-crystal, 1:1.1 stoichiometric mixtures of IFB and SYA was dispensed in a 100 mL glass reactor from Mettler-Toledo. Seventy grams of n-propanol/water mixture (95/5, w/w) were added to the reactor and the temperature was increased to 80 °C with an overhead stirrer at 150 rpm. Seeds of I-SYA (1:1) co-crystal obtained previously during screening were used to induce crystallization and added to the reactor after cooling down to 55 °C. Three temperature cycles from 55 °C to 15 °C were carried on with a cooling/heating rate of 0.1 K/min to promote crystal coarsening. A final cool down to 0 °C was done at 0.1 K/min. Solids were filtered, washed twice with 10 g of cold n-propanol/water mixture (95/5, w/w) and dried at 60 °C, 10 mbar for 24 h in a SalvisLAB vacuum dryer from Renggli (Rotkreuz, Switzerland) equipped with a Vacuubrand vacuum pump PC 2012 Vario CVC 2000 II (Theilingen, Switzerland).

The same procedure was used to prepare I-SYA (1:2) co-crystal salt with ten temperature cycles. This allowed conversion of the I-SYA (1:1) co-crystal to I-SYA (1:2) co-crystal salt. Imatinib hydrate (IH) was obtained from the precipitation of IM in 50 mM phosphate buffer at pH 6.8. Solids were filtered and gently dried at 30 °C, 30 mbar for 24 h in the vacuum dryer to preserve the hydrate. Subsequently a secondary drying was performed at 60 °C, 30 mbar for 24 h to induce the loss of water molecules. Hydrate formation and stoichiometry were investigated by DSC and TGA.

3.3. Single-crystal X-ray diffraction

Intensity data were collected at 100 K on a Bruker AXS three-circle diffractometer (Madison, WI) with monochromated Cu(K_α)-radiation (Helios MX confocal mirror monochromator), microfocus rotating anode generator, and a Smart 6000 CCD detector using the SMART software V5.632 from Bruker. 13 ω-scans at different φ-positions were performed to ensure appropriate data redundancy (4.7). Data processing and global cell refinement were performed with SAINT V7.36A from Bruker. A semi-empirical absorption correction was applied, based on the intensities of symmetry-related reflections measured at different angular settings (Sheldrick GM (2008) SADABS V2008/1, Bruker AXS Inc).

The structure was solved by dual space-recycling methods and subsequent DF syntheses and refined based on full-matrix least-squares on F2 using the SHELXTL program suite (Sheldrick GM (2001) SHELXTL V6.12, Bruker AXS Inc.). Anisotropic displacement parameters were used for all non-hydrogen atoms. Hydrogen atoms were located in DF maps and refined in idealized positions using a riding model.

3.4. X-ray powder diffractometry (XRPD)

Dried solids and wet residues from dissolution and solubility experiments were charged between thin-film SpectroMembrane of Kapton from Chemplex Industries (Palm City, FL) in a metallic holder and analyzed with a PANalytical X'Pert PRO powder diffractometer from PANalytical (Zürich, Switzerland) using Cu(K_α)-radiation (unsplit $K_{\alpha1}$ + $K_{\alpha2}$ doublet, mean wavelength 1.5419 Å) at a power of 40 kV and 40 mA, and a focusing X-ray mirror for Cu radiation. The scattered X-ray went through a 0.04 rad axial Soller slit and a 2.5 mm anti-scattering slit and detection was performed with an X'Celerator detector from PANalytical. Measurements were done in transmission mode in coupled two theta/theta mode with a step size of 0.0084° in 2θ and 25 s measurement times per step in the range of 4–40° (2θ). Data analysis was carried out with the software Data Viewer from PANalytical.

3.5. Differential scanning calorimetry (DSC)

DSC was performed on a Q2000 instrument from TA Instruments (New Castle, DE) using a scanning rate of 20 K/min from 25 to 250 °C for the IFB, IM, IH; and from 25 to 200 °C for the I-SYA co-crystals, under a nitrogen purge (flow rate of 50 mL/min). Two to five mg of the samples was weighted into a non-hermetic closed aluminum crucible (Tzero Pan and Lid from TA Instruments).

3.6. Thermogravimetric analysis (TGA)

TGA of IH was performed on a Discovery TGA instrument from TA Instruments using a scanning rate of 20 K/min from 25 to 250 or 300 °C. Two to five mg of the samples was weighted in an aluminum cup (TA Instruments).

3.7. Buffer preparation

50 mM phosphate buffer pH 6.8 was prepared accordingly to the United States Pharmacopeia (USP) [20]. 0.9 g of sodium chloride and 6.8 g of potassium dihydrogen phosphate were dissolved in 950 mL of Millipore water. The pH was measured with a SevenCompact pH meter from Mettler-Toledo (Greifensee, Switzerland) equipped with an InLab Micro electrode and adjusted with 1 M HCl or NaOH of Titripur grade from Merck (Darmstadt, Germany), if necessary. Then the volume was adjusted to 1 L.

3.8. Solubility measurements

The equilibrium solubility of IFB in phosphate buffer at pH 6.8 was determined by the shake flask method. An excess of solids (5 mg/mL) was added to 3 mL of phosphate buffer and stirred with a magnetic stirrer for 24 h at room temperature. In addition the equilibrium solubility of IFB in physical mixtures with one and two molar equivalents of SYA was measured. After 24 h, the pH was recorded and the samples were filtered through 0.45 µm PVDF Ultrafree MC HV centrifugal filters from Merck & Cie (Schaffhausen, Switzerland) in a miniSpin centrifuge from Vaudaux-Eppendorf AG (Basel, Switzerland) at 13.400 rpm for 90 s. Filtrates were further diluted with acetonitrile, and the amount of Imatinib and SYA in solution was quantified by UPLC-UV. Excess solids remaining on the filters were analyzed by XRPD. All experiments were performed in triplicate.

3.9. Kinetic dissolution profile measurements

Fifteen or 30 mg of substance (equivalent to free base) were added to 3 mL of 50 mM phosphate buffer pH 6.8 (SIF) at room temperature. Stirring was done with a magnetic stirrer at 300 rpm. At predefined time points, 100 µL aliquots were sampled and filtered through 0.45 µm PVDF centrifugal filters from Ultrafree in a miniSpin centrifuge at

13.400 rpm for 90 s. Filtrates were diluted with acetonitrile and assayed by UPLC-UV. At the end of the experiment (24 h), solids were filtered and analyzed by XRPD. The pH value was recorded 3 h after the start of the experiments. For IFB no pH change was observed, for IM and I-SYA (1:1) co-crystal the pH changed slightly to 6.5 and for I-SYA (1:2) co-crystal salt decreased to 5.9. For SYA a pH of 5.0 was observed. All experiments were performed in triplicate.

3.10. Ultra performance liquid chromatography (UPLC)

Quantification for the solubility measurements was performed on a 1290 Infinity UPLC from Agilent Technologies (Basel, Switzerland) equipped with a diode array detector (G4212A), an auto sampler (G4226A), a column thermostat (G1330B) and a quaternary pump (G4204A) with an Acquity UPLC BEH C18 1.7 µm (2.1 × 100 mm) column from Waters (Milford, MA). Different methods were used for Imatinib and SYA. For the analysis of Imatinib, the column temperature was set to 35 °C. Mobile phase A was a 10 mM phosphate buffer prepared by dissolving 2.27 g of sodium phosphate monobasic monohydrate and 0.954 g of sodium phosphate dibasic heptahydrate in 2 L of Millipore water. The pH was checked with a SevenCompact pH meter from Mettler-Toledo (Greifensee, Switzerland) equipped with an InLab Micro electrode, and adjusted to 6.4 with 1 N HCl or NaOH solutions, if necessary. Mobile phase B was a mixture of acetonitrile and water (95/5; v/v). The gradient profile was as follows for mobile phase B: 0–5 min 10–90%; 5–5.25 min 90%; 5.25–5.50 min; 90–10%; 5.50–6.50 min 10%. The flow rate was set at 0.6 mL/min and detection was performed at λ = 267 nm. For the analysis of SYA the UPLC method was modified. The temperature of the column oven was increased to 40 °C and the mobile phase consisted of 0.1% formic acid in Millipore water (A) and (B) of a mixture of acetonitrile and water (95/5; v/v). The gradient profile was as follows for mobile phase B: 0–5 min 10–90%; 5–5.25 min 90%; 5.25–5.50 min; 90–10%; 5.50–6.50 min 10%. The flow rate was set at 0.6 mL/min and detection was done at λ = 275 nm.

3.11. High performance liquid chromatography (HPLC)

Quantification of Imatinib and SYA in the Caco-2 permeation assay was performed on a LaChrome Ultra HPLC from Hitachi (Tokyo, Japan) equipped with two L160U Pumps, L-2200U Auto sampler, L-2300 Column oven and a L-2455U DAD detector with a ZORBAX Eclipse XDB-C18 5 µm (4.1 × 150 mm) column from Agilent. Mobile phases were 5 mM sodium dodecyl sulfate (SDS) in water and acetonitrile (90/10; v/v) adjusted to pH 2.3 (A) and 5 mM SDS in water and acetonitrile (10/90; v/v) (B). The temperature of the column oven was set to 20 °C, with a flow of 1 mL/min, an injection volume of 20 µL and a detection wavelength of λ = 267 nm. The gradient profile was as follows for mobile phase B: 0–3 min 20%; 3–7 min 20–90%, 7–10 min 90%, 10–11 min 90–20%, and 11–12 min 20%.

Propranolol analysis was performed with a ZORBAX Eclipse XDB-C8 5 µm column (4.6 × 150 mm) from Agilent at 35 °C with UV detection at λ = 292 nm. The injection volume was 20 µL and the flow of the mobile phase was set to 1 mL/min. The mobile phase consisted of 20 mM ammonium acetate buffer at pH 3.5 (A) and acetonitrile (B). The gradient profile was as follows for mobile phase B: 0–2 min 30%; 2–5 min 30–70%, 5–5.5 min 70%, 5.5–5.6 min 70–30%, 5.6–6 min 30%.

3.12. Nuclear magnetic resonance experiments

A 50 mM buffer with of dibasic sodium phosphate in D_2O was prepared and the pH was adjusted with NaOD or D_3PO_4 to pD 7.81 (=pH 7.4). The critical aggregation concentration (CAC) was determined by ^1H NMR concentration dependent measurements as previously described [21]. The supersaturated state was simulated by increasing the nominal concentration to 1000 µM Imatinib. Briefly, 100 mM stock solutions of IM, IFB, I-SYA (1:1) co-crystal and I-SYA

(1:2) co-crystal salt, respectively, in DMSO-d_6 was prepared and 15 μL was added to 1500 μL buffer (solvent switch method). The following dilution scheme was used (1000 μM; 1000 μM + surfactant (tween 80); 500 μM; 250 μM; 125 μM; 62.5 μM). The concentration dependent ^{1}H NMR spectra were recorded on a Bruker Avance 400 MHz spectrometer (Karlsruhe, Germany) operating at 400.13 MHz with a BBO BB-H 5 mm probe head, and data processing was done with the software TopSpin 3.0. The temperature was adjusted with a BCU-05 (Bruker) temperature control unit. The following acquisition parameters were applied for the ^{1}H NMR: number of scans 1024, at a temperature of 300 K, flip angle 30°, spectral width 20.55 ppm, and transmitter offset at 6.175 ppm. The acquisition time was set to 3.985 s followed by a relaxation delay of 1.0 s with collection of 64,000 data points at a sample spinning frequency of 20 Hz. Processing was done using an exponential line broadening window function of 0.3 Hz, automatic baseline correction and manual phasing. The spectra were referenced to the external standard 0.05% sodium trimethylsilylpropionate in D_2O (TSP-d_4) filled in a coaxial insert tube.

2D ROESY spectra were recorded with a Bruker 600 MHz Avance III HD NMR spectrometer using a 5 mm cryo-probe and the pulse sequence roesyphpp.2 in the phase-sensitive mode with cw spinlock for mixing and a purge pulse before d1 to avoid TOCSY cross peaks. A manual phase correction and an automatic baseline correction in both dimensions were performed.

For the ROESY experiments the 1000 μM I-SYA (1:2) co-crystal salt sample in deuterated buffer pH 7.4 was degassed by three freeze-thaw cycles filled in a 5 mm LPV tube from Wilmad-LabGlass, (Vineland, NJ) and measured after preparation i.e. in supersaturated state and after 72 h (in equilibrium).

3.13. Permeation study

In vitro permeation studies were carried out using Side-Bi-Side Cells from PermeGear, (Hellertown, PA) consisting of 3.4 mL donor and acceptor compartments and a 0.9 mm orifice diameter. The cells were placed on a 9-Station Horizontal Cell Stirrer from SES GmbH (Bechenheim, Germany). Artificial membranes (PVDF, polyvinylidene fluoride, 0.45 μm, 0.78 cm^2) were purchased from Pion (Billerica, MA) and loaded with 25 μL of GIT lipid purchased from Pion. Temperature was at 37 °C throughout the experiment. The membranes were mounted between the two compartments and pre-heated phosphate buffer (37 °C) was added to the acceptor compartment. 100 μM (equivalent to Imatinib free form) clear solutions of IFB, IM, I-SYA (1:1) co-crystal and I-SYA (1:2) co-crystal salt were transferred into the donor compartment. Clear solutions were chosen instead of suspensions to control for the amount of Imatinib in solution. The maximum concentration of IFB in the acceptor compartment was 10 times below its equilibrium solubility, thus ensuring sink conditions. At predefined time points 50 μL aliquots were sampled from the acceptor compartment, diluted with acetonitrile and analyzed by UPLC-UV. All experiments were performed in triplicate. To investigate the difference between Imatinib and SYA, a solution of I-SYA (1:1) of 10 mM was used to allow quantification of SYA in the acceptor compartment (given the low permeability of SYA, the amount diffused from a 100 μM solution was below the limit of detection by UPLC-UV).

3.14. Caco-2 permeation assay

The Caco-2 permeation assay was performed in apical-basolateral direction as described before [22], and cells of passage 51–55 were used [n = 4]. In brief, cells were incubated in culture medium (DMEM high glucose, 10% (v/v) FBS and 1% (v/v) non-essential amino acid solution) at 37 °C, 5% CO_2. Four passages were necessary to develop the phenotype performed at 80% confluence in 1:4 ratios. Afterwards cells were seeded into the trans-wells at a density of 2.6×10^5 cells cm^{-2} and maintained for at least 21 days. Culture medium for maintenance

(DMEM high glucose, 10% (v/v) FBS, 1% (v/v) NEAA, 1% (v/v) penicillin G/streptomycin solution) was changed every other days. Transepithelial electric resistance (TEER) values were measured with an EVOM2 STX3 chopstick electrode connected to an EVOM2 epithelial voltammeter from World Precision Instruments (Sarasota, FL). HBSS at pH 7.4 was used as transportation medium and altered by adding 25 mM 2-(4-(2-Hydroxyethyl)-1-piperazinyl)-ethansulfonic acid (HEPES) and 0.35 g L^{-1} NaHCO$_3$. Stock solutions of all substances were prepared in DMSO and diluted with transportation medium resulting in test solutions of 100 μM with a maximum of 0.5% DMSO in all cases. Propranolol, Fluorescein and Lucifer Yellow solutions were used as controls. Trans-wells were washed with HBSS, removing residual culture medium, and 0.45 mL of test solution was applied in the apical chamber (donor). The basolateral chamber was filled with 1.2 mL HBSS (acceptor). Immediately after apical application, 0.05 mL was withdrawn from the donor chamber to determine the initial concentration. The plates were incubated at 37 °C, 0% CO_2 under gentle shaking and 0.25 mL samples were withdrawn from the receiving chamber after 30, 60, 90, 120, 150 and 180 min and immediately replaced with transportation buffer. Additionally after 180 min a 0.1 mL sample was taken from the apical chamber to calculate the mass balance. TEER values were measured directly before and after the experiment to monitor the integrity of the monolayer [22]. Monolayers with a TEER value ≥ 200 Ω cm^2 were considered integer. Apical and basolateral samples were stored at −80 °C and analyzed by HPLC-UV (see below) for Propranolol, Imatinib and SYA respectively. Fluorescein and Lucifer Yellow were analyzed by fluorimetry (see below).

3.15. Fluorimetric analysis of fluorescein and lucifer yellow

Fluorescein analysis was performed on a 96-well plate reader LS50 B luminescence from Perkin Elmer (Waltham, MA). Parameters were set to extinction wavelength λ = 450 nm, extinction slit 2.5, emission wavelength λ = 514 nm, emission slit 15 and read time 0.4 s. A standard curve was determined between 1 μM and 0.05 μM (R^2 = 0.999). Lucifer Yellow analysis was performed on the same instrument. Parameters were set to extinction wavelength λ = 470 nm, extinction slit 2.5, emission wavelength λ = 535 nm, emission slit 2.5 and read time 5 s. A standard curve was determined between 10 μM and 0.1 μM (R^2 = 0.998).

4. Results and discussion

4.1. Structural studies

Imatinib and syringic acid (SYA) (Scheme 1) co-crystallized in the triclinic crystal system in the space group ($P\bar{1}$) with Z = 2 in a ratio of 1:1 (referred to as I-SYA (1:1) co-crystal, Fig. 1A, Table S1). The carboxylic function COOH (H 49) of SYA formed a hydrogen bond with the pyridine nitrogen (N 2) of Imatinib (d: 1.84 Å; θ: 173.4°) and the
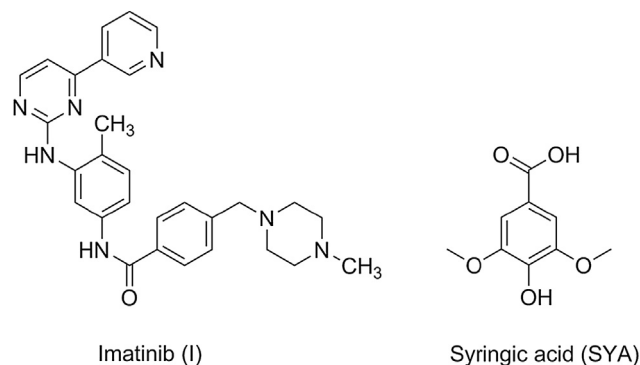
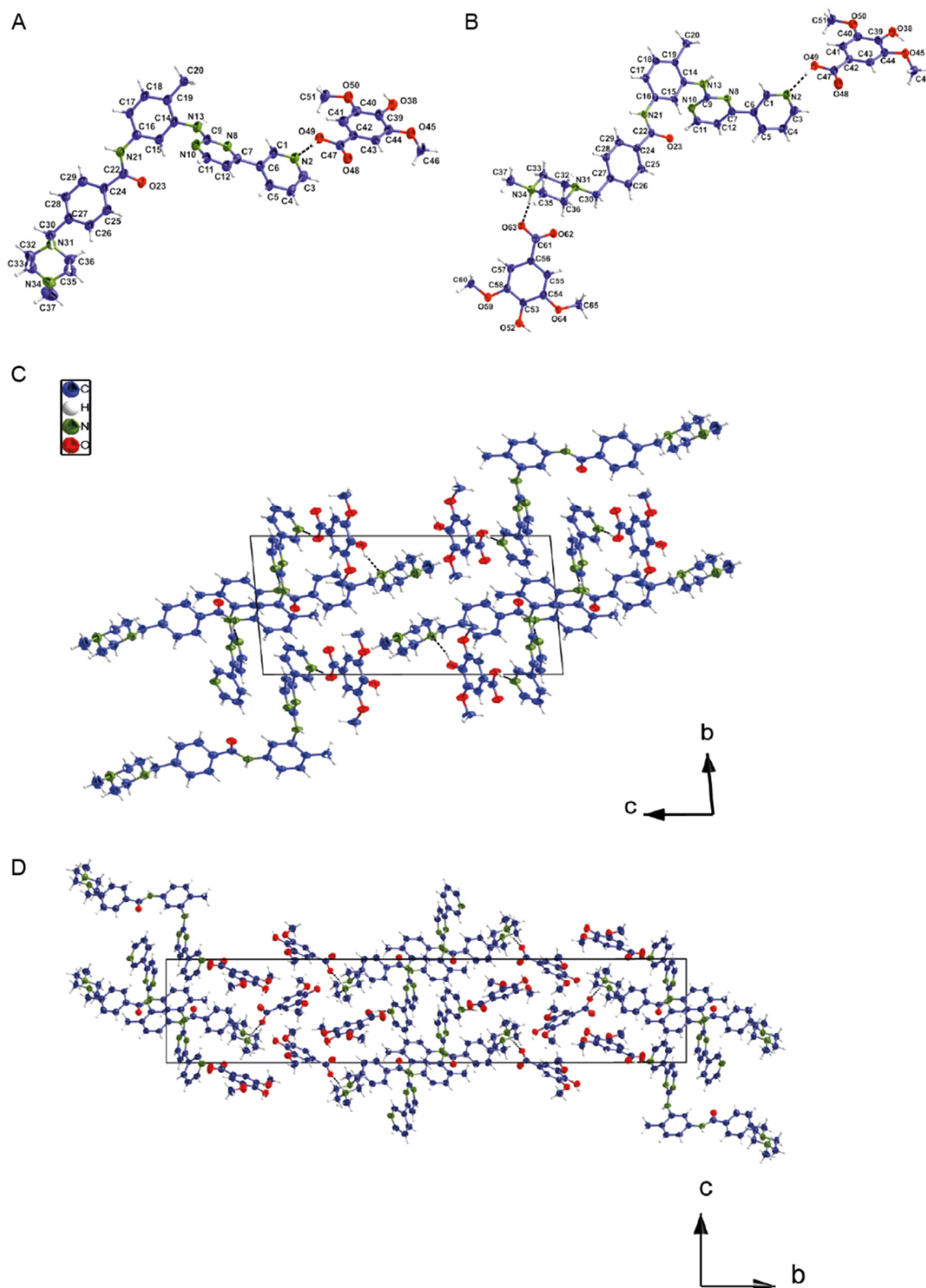**Scheme 1.** Structure of Imatinib (I) and syringic acid (SYA).

Fig. 1. (A) Crystal structure of the Imatinib syringate co-crystal I-SYA (1:1), and (B) the Imatinib syringate co-crystal salt I-SYA (1:2), (C) crystal packing of the Imatinib syringate co-crystal I-SYA (1:1), and (D) the Imatinib syringate co-crystal salt I-SYA (1:2).

hydroxyl group (H 38) of SYA with the piperazine nitrogen (N 31) of Imatinib (*d*: 2.00 Å; *θ*: 149.8°, Fig. 1C, Table S2). The Imatinib molecules adopted a head-to-tail conformation with hydrogen bonds between N−H 13 and O 23 (*d*: 2.11 Å; *θ*: 153.9°) and N−H 21 and N 10 (*d*: 2.24 Å; *θ*: 163.2°), and π stacking of the aromatic functions [23]

(Fig. 1C, Table S2).

Repeated cycles of heat and cool crystallization yielded a co-crystal salt of Imatinib and SYA with a ratio of 1:2 that crystallized in the monoclinic crystal system in the space group ($P2_1/c$) with Z = 4 (referred to as I-SYA (1:2) co-crystal salt, Fig. 1B, Table S1). The acid of the
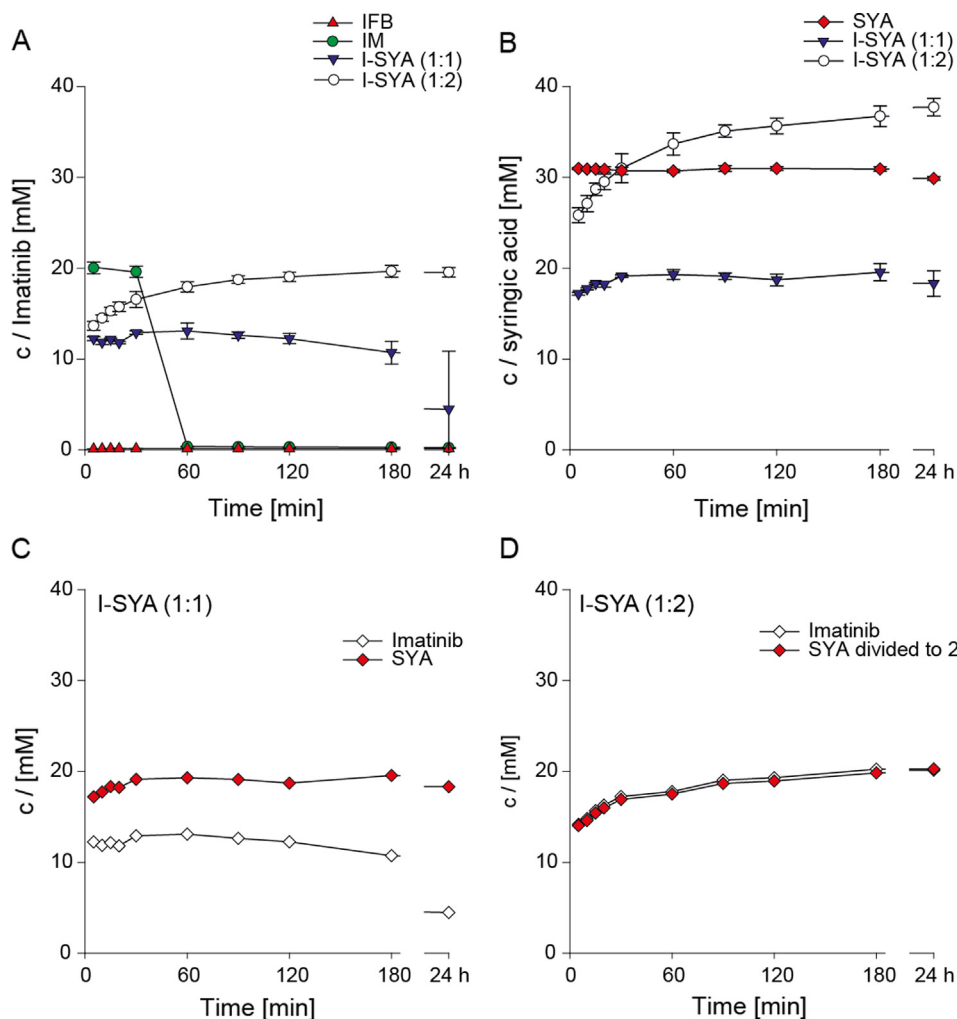
Fig. 2. Dissolution profiles of Imatinib free base (IFB), Imatinib mesylate (IM), Imatinib syringate co-crystal I-SYA (1:1) and Imatinib syringate co-crystal salt I-SYA (1:2) in simulated intestinal buffer at pH 6.8 (n = 3). (A) Imatinib concentrations, (B) Syringic acid (SYA) concentrations, (C) both concentrations in one plot for I-SYA (1:1) co-crystal and (D) for I-SYA (1:2) co-crystal salt.
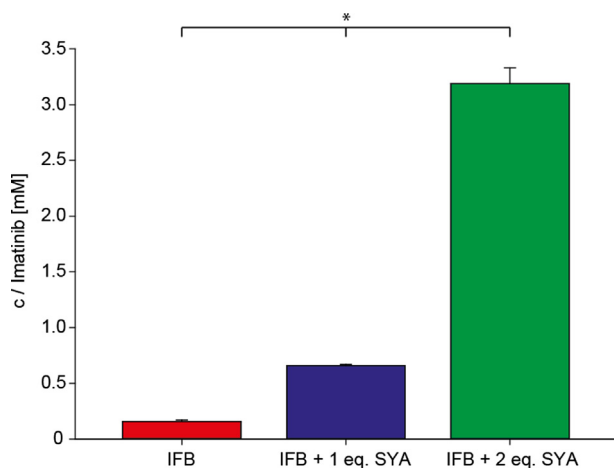

Fig. 3. Concentration of Imatinib in a physical mixture of Imatinib free base (IFB) with syringic acid (SYA) in the molar ratio 1:1 and 1:2 compared to IFB alone slurried in SIF buffer for 24 h.

first SYA molecule was activated as a carboxylate as the proton (H 63) was transferred to the piperazine nitrogen (N 34) of Imatinib (*d*: 1.76 Å; *θ*: 166.6°, Fig. 1B, Table S2), which yielded a salt. The second SYA molecule remained neutral and the same hydrogen bond between the

carboxylic group (H 49) of SYA and the pyridine nitrogen (N 2) of Imatinib as for the non-salt I-SYA (1:1) was observed (*d*: 1.92 Å; *θ*: 160.6°, Fig. 1B. Table S2). Imatinib molecules adopted the same head-to-tail conformation as observed for the I-SYA (1:1) co-crystal (Fig. 1D).

The C–O bond lengths of the SYA molecules in the crystal structure were in line with values found in the literature [24,25]. For the Imatinib syringate co-crystal I-SYA (1:1) a C–O bond length (C47–O48) of 121.7(5) pm was observed, which corresponds to a carboxylic acid. Also the C1–N2–C3 bond angle matched with literature values for a unprotonated pyridine nitrogen N2 [26]. In contrast for I-SYA (1:2) co-crystal salt the second C–O bond length (C61–O62) was 125.1(4) pm belonging to the carboxylate function of the deprotonated second SYA molecule.

Increasing SYA stoichiometry went along with an increased measured density (1.269, 1.299, and 1.369 g/cm^3 for IFB, I-SYA (1:1) and I-SYA (1:2), respectively, Table S1) which suggested lower lattice forces of the co-crystals. Both co-crystals were thin, long needles.

4.2. Thermal analysis

Both, the I-SYA (1:1) co-crystal and I-SYA (1:2) co-crystal salt had a melting point of 164 °C, which was lower than of Imatinib free base (IFB, 211 °C), Imatinib mesylate (IM, 219 °C), or SYA alone (208 °C) as determined by DSC (Fig. S1).
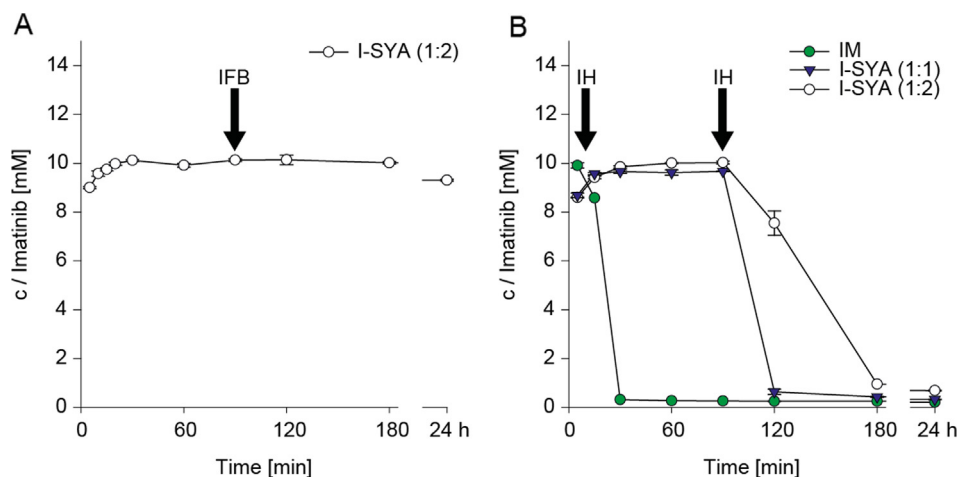
Fig. 4. (A) Seeding experiments of the Imatinib syringate co-crystal salt I-SYA (1:2) solution with Imatinib free base (IFB) seeds and (B) seeding experiments of Imatinib mesylate (IM), Imatinib syringate co-crystal I-SYA (1:1), and Imatinib syringate co-crystal salt I-SYA (1:2) solutions with Imatinib hydrate (IH) seeds.

4.3. Powder dissolution studies

Powder dissolution experiments were performed under non-sink conditions in simulated intestinal fluid (SIF) [20], a 50 mM phosphate buffer at pH 6.8 (Fig. 2). The IM salt dissolved rapidly generating a high concentration of Imatinib dropping within 1 h whereas IFB dissolved to a limited extend given its low thermodynamic solubility at neutral pH (Fig. 2A). I-SYA (1:1) co-crystal and I-SYA (1:2) co-crystal salt initial dissolution was slightly slower than the mesylate salt for the first 30 min, however high Imatinib concentrations were maintained for more than 3 h and 24 h, respectively. The collapse of supersaturation of IM and I-SYA (1:1) co-crystal resulted in a precipitate of Imatinib hydrate (IH) form as confirmed by XPRD (Figs. S3 and S4) and DSC/TGA data (Figs. S5 and S6), while SYA remained in solution (Fig. 2B).

In contrast to IM which directly precipitated into crystalline IH, liquid-liquid phase separation (LLPS) was observed for I-SYA (1:1) co-crystal. The amorphous, hydrophobic droplets were enriched with Imatinib (ratio 2.5:1; Imatinib to SYA, determined by UPLC analysis) with IH crystals occurring inside the droplets over time, while the surrounding aqueous, continuous phase was enriched with SYA (ratio 1:1.5; Imatinib to SYA). Due to concomitant LLPS, no congruency of the release of Imatinib and SYA from I-SYA (1:1) co-crystal was observed (Fig. 2C), while for I-SYA (1:2) co-crystal salt a congruent release of Imatinib and SYA was observed (Fig. 2D).

We further studied whether the increased kinetic solubility observed for the I-SYA co-crystals resulted from solubilization – SYA has structural analogy to known hydrotropic agents such as benzoic acid for which hydrotropic solubilization was reported [27,28] – or from a prevention of nucleation of the less soluble IH. This mechanistic understanding drives biopharmaceutical considerations in that transiently supersaturated and thermodynamically unstable solutions support the flux through membranes hence bioavailability, whereas thermodynamically stable, solubilized solutions might display a lower flux.

First, physical mixtures of IFB with one and two molar equivalents of SYA were slurried in SIF buffer for 24 h. At equilibrium, the amount of dissolved Imatinib was four and twenty times higher as compared to IFB with one and two molar equivalents of SYA, respectively (Fig. 3) and no change into hydrates was observed (Fig. S7). These results indicated that SYA could potentially – at least in part – act as a hydrotropic solubilizer for IFB.

In an effort to further understand the mechanism of supersaturation or solubilization, we seeded solutions of IM, I-SYA (1:1) co-crystal or I-SYA (1:2) co-crystal salt with either IFB or IH (Fig. 4). After seeding with IFB, the solution of I-SYA (1:2) co-crystal salt remained supersaturated (Fig. 4A) – however, when seeded with crystals of IH, all three

forms (IM, I-SYA (1:1), I-SYA (1:2)) rapidly precipitated as IH (Fig. 4B, Fig. S8). Therefore, SYA failed to solubilize IH, but delayed IH's nucleation. Hence when nucleation kicks in, SYA becomes powerless in preventing further crystal growth of IH.

4.4. ^{1}H NMR studies

We further studied molecular self-aggregation in solution by ^{1}H NMR [21,29]. Imatinib self-aggregated at pH 7.4, as indicated by concentration dependent shifts of the ^{1}H signals (critical aggregation concentration (CAC) $\approx$ 25–50 μM) for IFB, IM, I-SYA (1:1) co-crystal and I-SYA (1:2) co-crystal salt (Figs. S9–S12). Neither the methanesulfonic acid counterion nor the co-crystal former SYA prevented Imatinib aggregation in solution. Supplementation of a surfactant (tween 80) reverted the shifts for Imatinib reflecting the breakup of the Imatinib aggregates by the surfactant (Figs. S9–S12). Almost identical chemical shifts were observed for Imatinib's ^{1}H signals for IFB, IM and I-SYA (1:1) co-crystal, whereas for the I-SYA (1:2) co-crystal salt the signals were shifted to higher field when analyzed at the highest nominal concentration of 1000 μM (Figs. 5A and 6A). Sharp signals were recorded indicating a small size of the aggregates as of fast tumbling rate [21].

Similar to Imatinib, SYA displayed concentration dependent chemical shifts (CAC $\approx$ 25–50 μM) with sharp signals, but the aggregates did not respond to the supplementation of surfactant possibly reflecting aggregates with low aggregation numbers and similar hydrophilicity than SYA alone i.e. the surfactant was ineffective (Fig. S13). In presence of Imatinib the ^{1}H signals of SYA shifted to higher field in contrast to SYA alone (Fig. 5B), and the shifts for SYA reverted to the initial state for I-SYA (1:1) co-crystal and I-SYA (1:2) co-crystal salt upon surfactant supplementation (Fig. 6B) suggesting at least in part close arrangement of SYA molecules to Imatinib aggregates as the chemical shifts of SYA were affected by the ring current effects of Imatinib's aromates. The surfactant sensitivity of SYA only in presence of Imatinib molecules evidenced that the shifting of SYA's ^{1}H signals was a result of aggregation of Imatinib and not due a weak pH change.

In ROESY experiments no cross peaks between Imatinib and SYA molecules were observed (data not shown), suggesting that the intermolecular distance between SYA and Imatinib exceeded 3–5 Å [30]. As reported (*vide supra*) the IH form precipitated directly from IM but not from I-SYA (1:1) co-crystal solution for which LLPS was observed (Fig. 2) reflecting kinetically hindered displacement of the SYA molecules from Imatinib by water.

These results are in agreement of previous reports [8]. For example a furosemide co-crystal with 2-picolinamide was suggested to
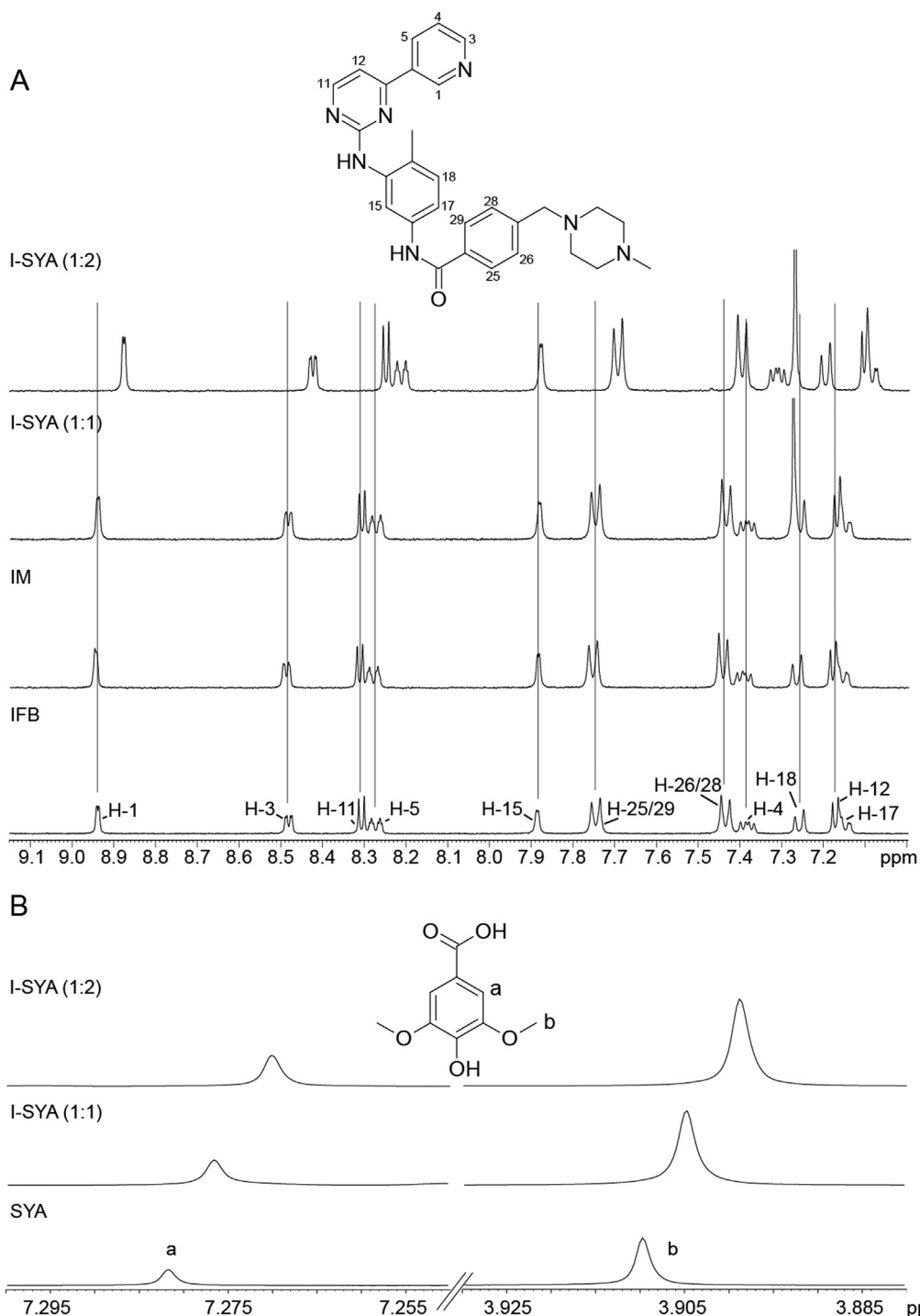
Fig. 5. (A) Aromatic range of the ^{1}H NMR spectra of Imatinib in 1000 μM solutions of Imatinib free base (IFB), Imatinib mesylate (IM), Imatinib syringate co-crystal I-SYA (1:1), and Imatinib syringate co-crystal salt (1:2), and (B) the ^{1}H signals of syringic acid (SYA) in SYA, I-SYA (1:1) and I-SYA (1:2) 1000 μM solutions in deuterated phosphate buffer at pH 7.4.

incompletely dissociate in solution thereby acting as a precipitation inhibitor delaying the nucleation of more stable polymorphs [12]. The term "synthon-extended-spring-and-parachute model" was coined to describe the persistence of synthons in solution, and their effect on precipitation of less soluble forms [12]. Imatinib contains several basic nitrogens which could form COOH···N or phenol OH···N heterosynthons with SYA. According to the above mentioned model, these supramolecular synthons could persist in solution and interfere with the rearrangement of Imatinib molecules into stable IH nuclei. In addition to intermolecular interactions, the amphiphilicity and hydrophobicity

of API and coformer might be important drivers of solution stability. For instance, previous work on amorphous liquids of the drug Selurampanel evidenced a systematic increase in supersaturation time with increasing hydrophobicity of the counterion [13]. The analysis of solution stability results found in the literature by Schultheiss et al. revealed that co-crystals with low solubility coformers tend to have better solution stability [31]. In the light of these pieces of work, amphiphilicity of co-crystal former and a moderate solubility appear to be important factors to limit dissociation upon dissolution, thus offering an effective solution to maximize the kinetic solubility of co-crystals of
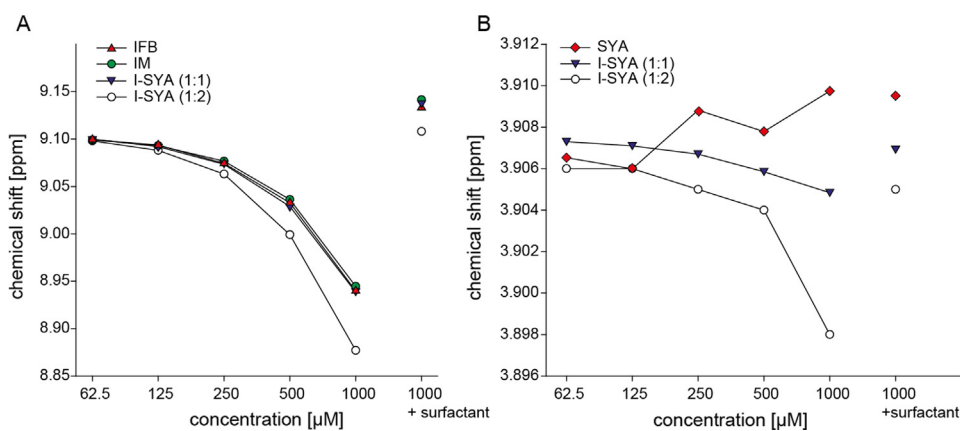
Fig. 6. Concentration dependent chemical shifts of the ^{1}H signals of (A) Imatinib (H-1) and (B) the methoxy groups of syringic acid (SYA). Additional to the nominal concentration of 1000 μM surfactant (tween 80) was added, which broke up the Imatinib aggregates indicated by the reversed shift.
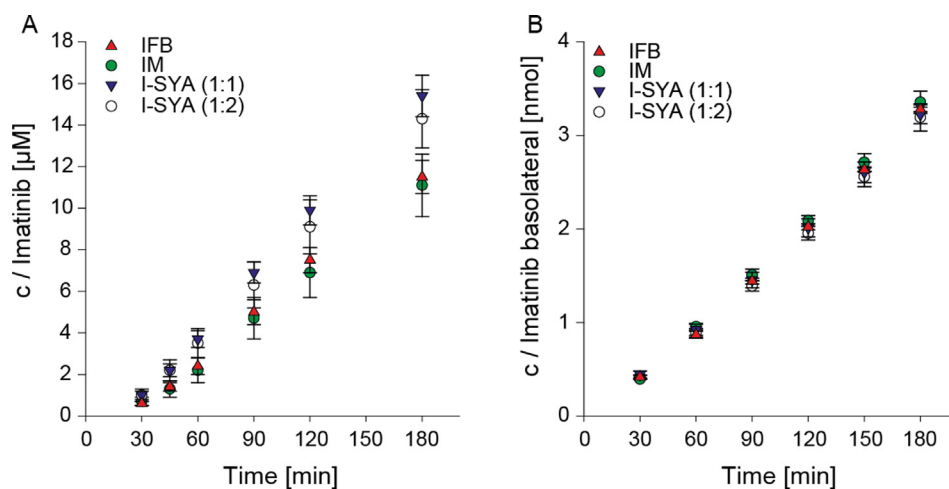

Fig. 7. Diffusion of Imatinib after application of 100 μM Imatinib free base (IFB), Imatinib mesylate (IM), Imatinib syringate co-crystal I-SYA (1:1) and Imatinib syringate co-crystal salt I-SYA (1:2) solutions (A) Artificial membrane (B) Caco-2 mono cell layer.

hydrophobic, poorly water-soluble APIs.

4.5. Permeation studies

The absorption of an API from the intestinal lumen compartment to the blood circulation results from its solubility and permeability. Since passive diffusion through artificial and biological membranes depends on activity and supersaturation gradients rather than on the total drug concentration [32,33], understanding if and how aggregation in solution impacts the thermodynamic activity and diffusion processes is important. In particular, questions arose whether (1) Imatinib and SYA crossed the membrane as aggregates (2) if so, were these aggregates as permeable as the free base and (3) if not, how relevant was the free drug concentration of Imatinib which existed in equilibrium to the aggregates?

For this, *in vitro* diffusive flux was studied between 30 min and 3 h, in order to account for the initial lag time, at identical concentrations among groups (100 μM equivalent Imatinib free base).

All groups diffused at comparable rates through an artificial membrane (Fig. 7A) or Caco-2 mono cell layers (Fig. 7B) indicating that neither the presence of SYA nor methanesulfonic acid impacted the permeability of Imatinib. Therefore, we speculate that the co-crystal approach enhanced diffusion by increasing local concentration at the barrier but co-permeation of the API and the counterion or coformer was unlikely. This was also reflected by Imatinib's concentration rising faster in the acceptor than that of SYA (Fig. S14) – similar conclusions

were done in previous reports [34].

No evidence was found that aggregates in solution prevented partitioning into the membrane, contrasting other studies reporting that the large size of colloidal species could prevent passive diffusion across cell membranes [35]. In fact, this might depend on the strength of the association between the species, on the affinity of each of the molecules to form aggregates, and on their individual partitioning into the membrane. In the present case the association between SYA and Imatinib was sufficiently diffuse to allow the free species independent diffusion. Likely, as monomers were in equilibrium with the aggregates, rapid dissociation of the aggregates resupplied monomers for further diffusion.

5. Conclusion

One co-crystal of Imatinib with SYA in the ratio 1:1, and one 1:2 co-crystal salt were crystallized and characterized by single crystal X-Ray diffractometry and thermal analysis. Non-sink dissolution studies in SIF buffer revealed that the SYA co-crystals maintained a higher concentration of Imatinib over time, as compared to the IM salt. This behavior was explained by an aggregation of Imatinib molecules with SYA molecules, acting as precipitation inhibitors and delaying rapid nucleation into the stable form, the hydrate. Permeation through artificial and cellular membranes was not impacted by aggregation nor by SYA or methanesulfonic acid. In conclusion, this study detailed the mechanism of Imatinib supersaturation through a metastable association with the

SYA coformer in solution. Further studies are needed to adequately incorporate this principle into an experimental dosage form and to assess the resulting *in vivo* pharmacokinetics of these dynamics of dissolution and solubility behavior of I-SYA co-crystals.

Acknowledgements and disclosures

Appendix A. Supplementary material

Supplementary data associated with this article can be found, in the online version, at https://doi.org/10.1016/j.ejpb.2018.05.012.

References

[1] H.D. Williams, N.L. Trevaskis, S.A. Charman, R.M. Shanker, W.N. Charman, C.W. Pouton, C.J.H. Porter, Strategies to address low drug solubility in discovery and development, Pharmacol. Rev. 65 (2013) 315–499.

[2] S. Cherukuvada, N.J. Babu, A. Nangia, Nitrofurantoin-p-aminobenzoic acid co-crystal: hydration stability and dissolution rate studies, J. Pharm. Sci. 100 (2011) 3233–3244.

[3] M.T. Hauser, M. Wink, Uptake of alkaloids by latex vesicles and isolated mesophyll vacuoles of chelidonium majus (Papaveraceae), Z. Naturforsch. (1990) 949–957.

[4] S.S.B. Mösli, T.W. Waldhauser, Compartmentation of caffein and related purine alkaloids depends exclusively on the physical chemistry of their vacuolar complex formation with chlorogenic acid, Phytochemistry 42 (1996) 985–996.

[5] K. Gorter, Beiträge zur Kenntniss des Kaffees. (Erste Abhandlung), Liebigs Ann. Chem. 358 (1908) 327–348.

[6] N. D'Amelio, G. Papamokos, J. Dreyer, P. Carloni, L. Navarini, NMR studies of hetero-association of caffeine with di-O-caffeoylquinic acid isomers in aqueous solution, Food Biophys. 10 (2015) 235–243.

[7] J.C. Torre, G.W. Schmidt, C. Paetz, M. Reichelt, B. Schneider, J. Gershenzon, J.C. D'Auria, The biosynthesis of hydroxycinnamoyl quinate esters and their role in the storage of cocaine in Erythroxylum coca, Phytochemistry 91 (2013) 177–186.

[8] N.J. Babu, A. Nangia, Solubility advantage of amorphous drugs and pharmaceutical cocrystals, Cryst. Growth Des. 11 (2011) 2662–2679.

[9] P. Sanphui, G. Bolla, A. Nangia, V. Chernyshev, Acemetacin cocrystals and salts: structure solution from powder X-ray data and form selection of the piperazine salt, IUCrJ 1 (2014) 136–150.

[10] A. Alhalaweh, H.R.H. Ali, S.P. Velaga, Effects of polymer and surfactant on the dissolution and transformation profiles of cocrystals in aqueous media, Cryst. Growth Des. 14 (2014) 643–648.

[11] K. Shiraki, N. Takata, R. Takano, Y. Hayashi, K. Terada, Dissolution improvement and the mechanism of the improvement from cocrystallization of poorly water-soluble compounds, Pharm. Res. 25 (2008) 2581–2592.

[12] M. Banik, S.P. Gopi, S. Ganguly, G.R. Desiraju, Cocrystal and salt forms of furosemide: solubility and diffusion variations, Cryst. Growth Des. 16 (2016) 5418–5428.

[13] J. Wiest, M. Saedtler, A. Balk, B. Merget, T. Widmer, H. Bruhn, M. Raccuglia, E. Walid, F. Picard, H. Stopper, W. Dekant, T. Luhmann, C. Sotriffer, B. Galli, U. Holzgrabe, L. Meinel, Mapping the pharmaceutical design space by amorphous ionic liquid strategies, J. Control. Release 268 (2017) 314–322.

[14] M. Yoshimura, M. Miyake, T. Kawato, M. Bando, M. Toda, Y. Kato, T. Fukami, T. Ozeki, Impact of the dissolution profile of the cilostazol cocrystal with supersaturation on the oral bioavailability, Cryst. Growth Des. 17 (2017) 550–557.

[15] I. Pasic, J.H. Lipton, Current approach to the treatment of chronic myeloid leukaemia, Leuk. Res. 55 (2017) 65–78.

[16] L.A. Pacheco-Palencia, S. Mertens-Talcott, S.T. Talcott, Chemical composition, antioxidant properties, and thermal stability of a phytochemical enriched oil from açai (Euterpe oleacea Mart.), J. Agr. Food Chem. 56 (2008) 4631–4636.

[17] W.R. Russell, L. Scobbie, A. Labat, G.G. Duthie, Selective bio-availability of phenolic acids from Scottish strawberries, Mol. Nutr. Food Res. 53 (Suppl 1) (2009) S85–S91.

[18] A. Ragusa, C. Centonze, M.E. Grasso, M.F. Latronico, P.F. Mastrangelo, F. Sparascio, F.P. Fanizzi, M. Maffia, A comparative study of phenols in Apulian Italian Wines, Foods 6 (2017) 24.

[19] R. Thipparaboina, S. Mittapalli, S. Thatikonda, A. Nangia, V.G.M. Naidu, N.R. Shastri, Syringic acid: structural elucidation and co-crystallization, Cryst. Growth Des. 16 (2016) 4679–4687.

[20] U.S. Pharmacopeia-National Formulary USP 41 NF 36 26th Edition, Rockville, MD, USA, 2018.

[21] S.R. LaPlante, R. Carson, J. Gillard, N. Aubry, R. Coulombe, S. Bordeleau, P. Bonneau, M. Little, J. O'Meara, P.L. Beaulieu, Compound aggregation in drug discovery: implementing a practical NMR assay for medicinal chemists, J. Med. Chem. 56 (2013) 5142–5150.

[22] I. Hubatsch, E.G. Ragnarsson, P. Artursson, Determination of drug permeability and prediction of drug absorption in Caco-2 monolayers, Nat. Protoc. 2 (2007) 2111–2119.

[23] D. Grillo, G. Polla, D. Vega, Conformational polymorphism on imatinib mesylate: grinding effects, J. Pharm. Sci. 101 (2012) 541–551.

[24] L. Leiserowitz, Molecular packing modes. Carboxylic acids, Acta Cryst. B, 32 (1976) 775–802.

[25] R. Taylor, O. Kennard, W. Versichel, The geometry of the N–H…O=C hydrogen bond. 3. Hydrogen-bond distances and angles, Acta Cryst. B, 40 (1984) 280–288.

[26] J.E. Del Bene, Molecular orbital study of the protonation of DNA bases, J. Phys. Chem. 87 (1983) 367–371.

[27] S.A. Damiati, L.G. Martini, N.W. Smith, M.J. Lawrence, D.J. Barlow, Application of machine learning in prediction of hydrotrope-enhanced solubilisation of indomethacin, Int. J. Pharm. 530 (2017) 99–106.

[28] V. Dhapte, P. Mehta, Advances in hydrotropic solutions: an updated review, St. Petersburg Polytech. Univ. J.: Phys. Math. 1 (2015) 424–435.

[29] S.R. LaPlante, N. Aubry, G. Bolger, P. Bonneau, R. Carson, R. Coulombe, C. Sturino, P.L. Beaulieu, Monitoring drug self-aggregation and potential for promiscuity in off-target in vitro pharmacology screens by a practical NMR strategy, J. Med. Chem. 56 (2013) 7073–7083.

[30] H. Friebolin, Ein- und zweidimensionale NMR-Spektroskopie, 4 ed., Wiley-VCH, Weinheim, 2006.

[31] N. Schultheiss, A. Newman, Pharmaceutical cocrystals and their physicochemical properties, Cryst. Growth Des. 9 (2009) 2950–2967.

[32] A.S. Indulkar, Y. Gao, S.A. Raina, G.G. Zhang, L.S. Taylor, Exploiting the phenomenon of liquid-liquid phase separation for enhanced and sustained membrane transport of a poorly water-soluble drug, Mol. Pharm. 13 (2016) 2059–2069.

[33] E. Borbas, B. Sinko, O. Tsinman, K. Tsinman, E. Kiserdei, B. Demuth, A. Balogh, B. Bodak, A. Domokos, G. Dargo, G.T. Balogh, Z.K. Nagy, Investigation and mathematical description of the real driving force of passive transport of drug molecules from supersaturated solutions, Mol. Pharm. 13 (2016) 3816–3826.

[34] A.O. Surov, T.V. Volkova, A.V. Churakov, A.N. Proshin, I.V. Terekhova, G.L. Perlovich, Cocrystal formation, crystal structure, solubility and permeability studies for novel 1,2,4-thiadiazole derivative as a potent neuroprotector, Eur. J. Pharm. Sci. 109 (2017) 31–39.

[35] S.C. Owen, A.K. Doak, A.N. Ganesh, L. Nedyalkova, C.K. McLaughlin, B.K. Shoichet, M.S. Shoichet, Colloidal drug formulations can explain "bell-shaped" concentration-response curves, ACS Chem. Biol. 9 (2014) 777–784.